Tutor/s
Dra. Laura Bayés García
Departament de Mineralogia, Petrologia i Geologia Aplicada
Dra. Mª Concepción López Martínez
Departament de Química Inorgànica i Orgànica

Grau de Química

Treball Final de Grau

Crystallization and polymorphism of blends based on cocoa butter and shea stearin for the development of novel lipid systems

Cristal·lització i polimorfisme de mescles de mantega de cacau i estearina de karité per al desenvolupament de nous sistemes lipídics

Alessandra Cutillo Foraster

June 2021

UNIVERSITAT DE BARCELONA
B:KC Barcelona Knowledge Campus
Campus d'Excel·lència Internacional

“Dinanzi ad un bivio di una strada che va in basso ed una che va in alto, prendi sempre quella che va in alto ti troverai sempre meglio.”

Tiziano Terzani

Agradezco a mi madre y a mi padre por permanecer siempre a mi lado, por apoyarme en cualquier decisión tomada y sostenerme en los momentos más difíciles. Sobretodo agradezco su apoyo durante la realización de todo el Grado de Química.

Agradezco a Laura Bayés García por haberme dado la oportunidad de realizar el proyecto de fin de grado con ella y su equipo y ayudarme, guiarme y aconsejarme para poder desarrollar un buen proyecto.

Agradezco a Jorge Macridachis González por ayudarme y aconsejarme durante la realización de los experimentos llevados a cabo en el proyecto de fin de grado.

Agradezco a Conchi López Martínez por los consejos dados para completar y perfeccionar el proyecto de fin de grado.

REPORT

CONTENTS

1. SUMMARY

Cocoa butter (CB) is a natural edible fat mainly composed of three main 1,3-disaturated-2-unsaturated triacylglycerols (TAGs): 1,3-dipalmitoyl-2-oleoyl-glycerol (POP), 1,3-distearoyl-2-oleoyl-glycerol (SOS), and *rac*-palmitoyl-stearoyl-2-oleoyl-glycerol (POS) and is responsible for the unique physicochemical properties of chocolate. In recent days, the increase in the demand for cocoa beans in the market has led to a rise in CB price, and for that reason the search for alternatives fats to CB is promoted. Some of these alternatives are Cocoa Butter Equivalents (CBEs), which usually are fat blends compatible with CB because of their similar physical and textural characteristics (melting, rheology, plasticity, etc.) compared to those of CB, and, generally, are obtained by blending fats rich in POP and SOS. One of the fats used as a source of SOS is shea butter from which shea stearin (ShS) is obtained by fractionation.

This work focuses on studying blends based on cocoa butter and shea stearin as a way to develop new lipid systems with improved properties for specific applications, and also to find out how ShS influences some properties of CB. To achieve all of these, in this research, the polymorphic and crystallization behaviour, the solid fat index (SFI), and the crystal morphology of CB, ShS, and some CB:ShS blends were investigated through differential scanning calorimetry (DSC), X-ray diffraction (XRD), and polarized light microscopy (PLM) techniques.

Keywords: cocoa butter, shea stearin, polymorphism, differential scanning calorimetry, X-ray diffraction, polarized light microscopy, solid fat index.

2. RESUM

La mantega de cacau (CB) és un greix natural, responsable de les propietats úniques de la xocolata (perfil de fusió, propietats texturals, reologia, plasticitat, etc.), que es constitueix principalment per tres triacilglicerols: 1,3-dipalmític-2-oleic-glicerol (POP), 1,3-diesteàric-2-oleic-glicerol (SOS) i *rac*-palmític-esteàric-2-oleic-glicerol (POS). En l'actualitat, l'increment en la demanda de les faves de cacau en el mercat s'està traduint en un augment del preu de la mantega de cacau, i és per aquest motiu que, s'ha impulsat la cerca de greixos alternatius, com els *Cocoa Butter Equivalents* (CBEs), els quals normalment consisteixen en mescles de greixos compatibles amb la mantega de cacau, gràcies a la similitud que presenten tant en composició, com en les propietats fisicoquímiques. D'entre ells, destaca la mantega de karité degut al seu elevat contingut en SOS, i d'ella se n'extreu l'estearina de karité (ShS) mitjançant processos de fraccionament específics.

Aquest treball es centra en l'anàlisi de mescles constituïdes per mantega de cacau i estearina de karité amb el propòsit de desenvolupar nous sistemes lipídics amb propietats millorades per a determinades aplicacions, i també determinar la influència de l'estearina de karité en les propietats fisicoquímiques de la mantega de cacau. Amb aquest objectiu, el comportament cristal·lí i polimòrfic, l'índex de greix sòlid i la morfologia cristal·lina de la CB, ShS i d'algunes mescles de CB:ShS han estat analitzats mitjançant les tècniques de calorimetria diferencial de rastreig (DSC), difracció de raigs X (XDR) i microscòpia de llum polaritzada (PLM).

Paraules claus: mantega de cacau, estearina de karité, polimorfisme, calorimetria diferencial de rastreig, difracció de raigs X, microscòpia de llum polaritzada, índex de greix sòlid.

3. INTRODUCTION

The polymorphism is defined as "a solid crystalline phase of a given compound resulting from the possibility of at least two different arrangements of the molecules in the solid state" [1]. The polymorphic behaviour of samples depends on molecular structure, thermodynamic stability, and phase transformation, and affecting their properties and potential applications.

It is well known that lipids are used as lipophilic materials in food, cosmetic and pharmaceutical industries [2]. Edible fats and oils (i.e. vegetable oils, margarine, chocolate, and confectionery fats) are formed by triacylglycerols (TAGs), which consist of triesters of a glycerol structure and three fatty acids (Figure 1). The physical properties of TAGs, such as melting, morphology, rheology and texture, are determined by fatty acid compositions (e.g. saturated/unsaturated acyl chains, unsaturated acyl chains with cis- or trans- double bonds, acyl chain length, etc) and their polymorphism [3]. TAGs can be divided into *mono-acid* or *simple* TAGs, which contain identical acyl chains in all positions, and *mixed-acid* TAGs, which have different acyl chains [4].

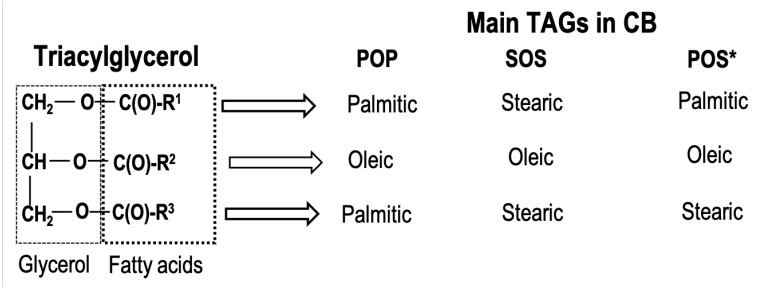

Figure 1. TAGs structure and the main TAGs in CB. POS* is a racemic TAG.

Cocoa butter (CB) is a natural edible fat, mainly composed of the three TAGs shown in Figure 1. CB is present in chocolate and confectionery products and has a major influence on their organoleptic and physical properties [5] (i.e. unique sensory characteristics related to gloss, texture, and typical melting behaviour of this product [6]).

The annual increase in the demand for chocolate and chocolate-type products is leading to an increase in the demand for cocoa beans. Hence, the varying supply and increasing price of CB depends on fluctuations of cocoa bean prices in the market [6]. For that reason, the search and development of cocoa butter alternatives (CBAs) is one of the challenges of food industry. Based on their composition (presence or absence of lauric acid arrays) and main TAGs contained, and also their compatibility with CB, the CBAs can be classified in three main categories shown in Figure 2 [5, 6] of which only cocoa butter equivalents (CBEs) (commonly produced by blending POP-rich fats (i.e. palm mid fraction), and lipids rich in SOS, like shea and kokum butters, show a total compatibility with CB.

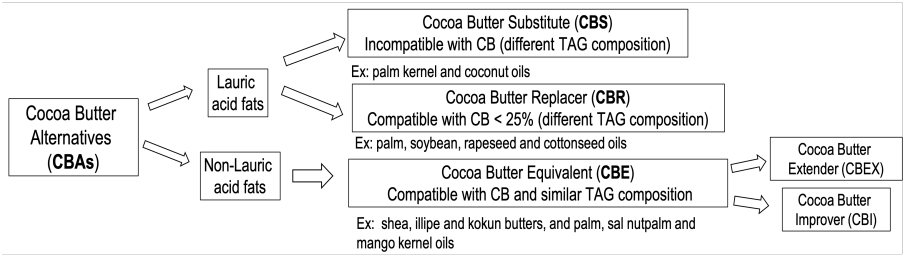

Figure 2. Classification of CBAs.

CBEs are further classified in a) cocoa butter extenders (CBEXs), that are lipid systems able to extend or dilute CB with the aim of making its use more economical, and b) cocoa butter improvers (CBIs), which are fats that improve the properties of chocolate or CB and typically have a high amount of SOS – TAG (Figure 1) [7]. Its presence in CBIs increases the solid fat content (SFC), the melting point, and the hardness of chocolate [6].

Despite the first studies on CB polymorphism were reported in 1966 [8], the interest on this topic has increased. Many studies on the CB polymorphism have been carried out [9, 10, 11], and its main TAGs, which are POS, POP, and SOS [12, 13]. For example, Bayés-García et al. [11] studied the crystallization and polymorphism of CB in bulk state and in fresh cacao beans of different geographical origins with DSC and X-ray diffraction techniques at different cooling and heating conditions, with a main objective of determining the necessary conditions of germination of cacao beans, which are strongly related to the crystallization processes of CB.

Shea stearin (ShS) is a lipid fraction rich in SOS, obtained from shea butter, a popular fat extracted from shea fruit of *Butyrospermun parki,* which is a tree indigenous of West Africa [14]. ShS is compatible with natural CB and, for that reason, it can be used as component of CBE in

chocolate formulation [14]. The polymorphic and crystallization studies of ShS are less common. Ray et al. [14] investigated the crystallization and polymorphic behaviour of ShS through measurements of SFC profile via pulsed NMR, variable temperature powder X-ray diffraction (XRD), polarized light microscopy (PLM), confocal Raman microscopy, and non-isothermal, isothermal and, "stop and return" differential scanning calorimetry (DSC). They also removed a small amount of diacylglycerols (DAGs) and oxidized material from ShS by a pre-treatment with silica and performed the same measurements used in ShS to understand the effects of minor components in the crystallization and polymorphic behaviour of ShS.

The studies of blends based on CB and ShS are extremely scarce. As far as we know, only two papers have been reported [15, 16]. Kang et al. [15] investigated fatty acid and TAGs compositions, crystallization and melting behaviour, and SFC of mixtures based on CB and CBE obtained by blending fractioned palm stearin and shea stearin. The aim of this work was to determine the appropriate amount of CBE to be blended with CB without significantly modify their physical properties. By contrast, Zeng et al. [16] studied the changes in solid fat content (SFC) of CB:ShS mixtures to evaluate the possibility of using shea stearin as CBE. In addition, an emulsifying compound was added to the blends, and they were characterized by sensory evaluation and texture profile analysis (TPA) in order to find the optimal emulsifying compound that improved taste and texture.

Despite the increase in new lipophilic materials as CB alternatives compatible with the properties of ShS (high content of SOS and compatible with CB), studies on CB and ShS mixtures have not been studied in detail and the influence of their composition, on their properties and behaviour still remains unknown.

TAGs exhibit complicated polymorphic structures and transformation pathways because of the diversity in their chemical structures [4]. The three typical polymorphic forms of TAGs are α, β' and β [17]. These polymorphic forms are defined based on their subcell structures (Figure 3), which correspond to cross-sectional packing modes of the zigzag aliphatic chain. Hence, α form is defined by a hexagonal subcell (H), β' has an orthorhombic perpendicular subcell ($O_{\perp}$), and the subcell β form is triclinic parallel ($T_{//}$).

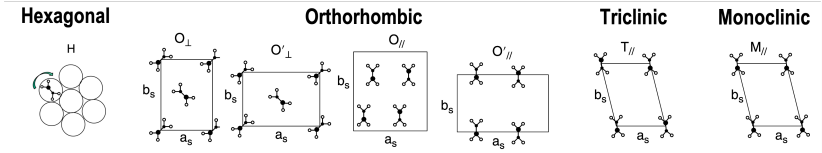

Figure 3. Subcell structures of TAGs. Adapted with permission from [4], © 2018 Willey Blackwell.

The subcell concept is often used to define hydrocarbon packing modes of lipids, where three axes, which are c_s related to the translation between equivalent positions within a chain, and a_s and b_s for the lateral translations, and three interaxial angles, mark the limits of the three-dimensional subcell. In the hexagonal subcell (H), commonly found in α form, the hydrocarbon chains freely rotate about their long axis, like in rotator phases of paraffins. Additionally, the parallel (//) and perpendicular (⊥) orientations are the two possibilities for the mutual orientation of zigzag planes designated by neighbouring hydrocarbon chains. For example, the parallel orientation is found in the triclinic parallel subcell ($T_{//}$) that are related to β polymorphic form and the perpendicular in the orthorhombic perpendicular (O⊥) associated to β' form [18].

Regarding to their relative stability, α form is the least stable and, therefore, that with the lowest melting temperature (T_m), β' form is also metastable, and β form is the most stable one. However, these basic polymorphic forms can be modified based on the fatty acid compositions and, consequently, new forms such as γ, δ or multiple β' forms can occur [19].

In the crystal, TAG molecules had a layer structure due to the strong interaction existing along lateral directions, consequently, bilayer o trilayer structure commonly can occur. A double chain length or bilayer structure (2L) is obtained when the chemical properties of the three fatty acid moieties are equal or very similar (Figure 4). On the contrary, a triple chain length or trilayer structure (3L) is formed when the chemical properties of one or two of the three chain moieties are considerably different from the other because of chain sorting (Figure 4) [20].

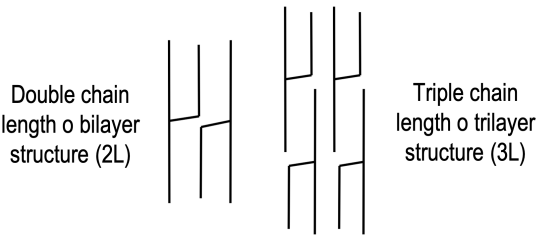

Figure 4. Chain length structure of TAGs. Adapted with permission from [4], © 2018 Willey Blackwell.

X-ray diffraction (XRD) allows to identify the polymorphic forms of TAGs using Bragg's law [4]. The short spacing values or wide-angle region diffraction peaks indicate the type of subcell present. Figure 5 shows typical XRD patterns associated to short spacing values of main polymorphic forms of TAGs [4]. As opposite, the long spacing values or small-angle region provide information related to chain length structure, that is to say if the polymorphic form has a triple chain length (3L) or double chain length (2L) structure.

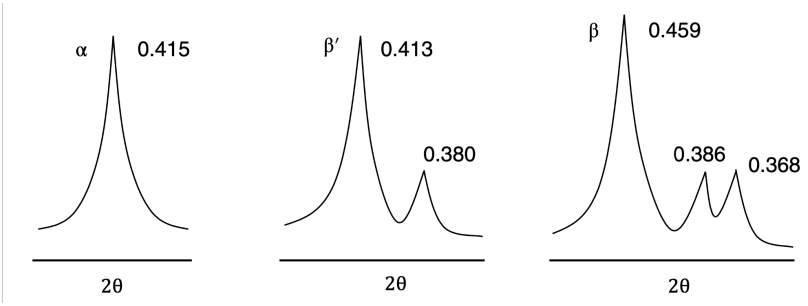

Figure 5. Typical short spacing values of α, β' and β polymorphic forms. D-spacing values are in nm. Reproduced with permission from [4], ©2018 Willey Blackwell.

The crystallization and polymorphic behaviour in lipid systems can become highly complex. As an example CB crystals exhibit six different polymorphic forms, Form I to Form VI. Among them, Form V is industrially promoted, as it provides the desired mouthfeel, sharp melting, and characteristics gloss and snap of chocolate. In the appendix 1, Table 1 shows typical long and short spacing values for each polymorph of CB, their melting temperature (T_m), and the equivalence with TAGs nomenclature in Greek letters [8]. As far as we know, the polymorphic forms of ShS have not been investigated in detail. For this reason, the polymorphic forms of SOS are used to interpret the results that will be obtain in this work (Table 2 in appendix 1) [12].

Although, the increasing interest in new lipophilic materials as potential CB alternatives, the nature of ShS (lipid system rich in SOS) and its high compatibility with CB, the polymorphic behaviour of CB:ShS blends have not been investigated, and the influence of their composition, on their properties and behaviour still remains unknown.

In this study, the polymorphism of CB, ShS, and some of its blends have been analysed by mainly using differential scanning calorimetry and X-ray diffraction when dynamic thermal treatments, based on the variation of the cooling and heating rates, were applied. Furthermore, the solid fat index (SFI) has been determined for all the samples as a function of temperature.

Polarized light microscopy (PLM) was also used to describe the microstructure exhibited by the samples at a certain temperature and time, and results were supported by corresponding XRD measurements.

4. OBJECTIVES

The main objective of this work is to carry out a comparative study of pure samples of CB, ShS, and blends based on different CB and ShS compositions under identical experimental conditions in order to develop new lipid systems with improved properties for specific applications in food products. Additionally, this study is complemented with crystal morphology and the evolution of solid percentages as a function of temperature through the solid fat index analysis.

5. EXPERIMENTAL SECTION

5.1. SAMPLES

CB used was provided by *Cacao Barry* (Gurb, Barcelona, Spain), and ShS was donated by *Lipidos Santiga S.A.* (Santa Perpetua de Mogoda, Barcelona, Spain). Table 1 shows the blends based on CB and ShS studied in this work. In order to ease the interpretation of the results, parallel studies of pure samples of CB and ShS under identical experimental conditions were carried out. All samples were stored in N_2-purged vials in the freezer. Before carrying out experiments, samples were melted at 70 ºC in a water bath and then mixed with a vortex to ensure that all crystal memory was removed.

Identification of blends	**A**	**B**	**C**	**D**	**E**
Composition	95CB:5ShS	80CB:20ShS	70CB:30ShS	50CB:50ShS	30CB:70ShS

Table 1. Blends based on CB and ShS studied in this work.

5.2. DIFFERENTIAL SCANNING CALORIMETRY

Differential scanning calorimetry (DSC) was used to study the thermal behaviour of the samples. DSC were conducted at atmospheric pressure using a *PerkinElmer Diamond* instrument. Samples (5 µL) were weighted into 50 µL aluminium pans, and covers were sealed into place. The instrument was calibrated using as a reference the enthalpy and the melting points of indium (T_m = 156.6 °C; ΔH = 28.45 J/g) and decane (Tm = -29.7 °C; ΔH = 202.1 J/g) standards. The reference used was an empty pan. Dry nitrogen was used as purge gas in the DSC cell at a flow rate of 20 cm^3/min. DSC thermograms were analysed using Pyris software to obtain the enthalpy (J/g) through the integration of the DSC signals, and temperature values of peaks observed in DSC (T_{top}, T_{onset} and $T_{end,}$ °C) by the intersections of the baseline and the initial and final tangents at the transition. All samples were subjected to a cooling process from 70 °C to -30°C at 2 ºC/min, and heating from -30 ºC to 70 ºC at the same rate. Additionally, CB, ShS, and **C**, **D** and **E** blends were also subjected to cooling and heating rates of 0.5 ºC/min. Three independent measurements were made for each cooling/heating conditions at 2 ºC/min. But for 0.5 ºC/min experiments were run in duplicates due to time restriction and an unexpected failure of the DSC instrument. Random uncertainty was estimated with 95 % threshold of reliability using the Student's method. For cooling and heating rates of 0.5 ºC/min a correction was applied (described in reference [21]).

DSC data were also used to predict the solid fat index (SFI) of the samples as a function of temperature. DSC heating curves were analysed to obtain total and partial enthalpies. The first SFI values were taken at a temperature of 5 ºC, where it was supposed that all the sample was in the solid state, and SFI was obtained for integration each 2 ºC interval until 37 ºC or 38 ºC, temperature at which it was estimated that the sample melted. However, the determination of SFI for the **E** blend and pure ShS was made manually due to the presence of exothermic peaks in the corresponding DSC thermograms, as only endothermic phenomena may be considered.

5.3. X-RAY DIFFRACTION

This technique was used to determine the occurrence of polymorphic forms when different thermal treatments were applied to lipid samples. Experiments were carried out through a PANalytical X'Pert PRO MPD 0/0 powder diffractometer with a radius of 240 mm, in a configuration of convergent beam with a focalizing mirror and a transmission geometry with a spinner glass capillary sample holder and equipped with a PIXcel detector (active length =

3.347º). The equipment also incorporated an Oxford Cryosystems 700 series Cryostream liquid nitrogen cryostat, enabling temperature control of the analysed capillary sample from 90 to 500 K. The radiation selected was monochromatic Cu $K\alpha_1$ (λ = 0.15418 nm). The sample was introduced in a 1.0 mm-diameter Lindemann glass capillary, which was rotated about its axis during the experiment to minimize preferential orientations of the crystallites. The step size was 0.026º 2θ and 2θ scans from 1º to 28º. The measuring time was 30 seconds per step. The XRD data were analysed using X'Pert HighScore software.

5.4. POLARIZED LIGHT MICROSCOPY

Crystal morphology was observed using a KERN OPO-1 polarized light microscope (KERN and Sohn GmbH, Balingen, Germany) linked to a KERN ODC 832 camera (KERN and Sohn GmbH, Balingen, Germany). Samples were melted at 70 ºC and a drop was placed on a preheated microscope glass slide. Then, a preheated cover slip was placed on top of the sample. Samples were transferred to an incubator at 22 ºC and temperature was maintained for 1, 5, 10, 20, 30, and 40 days. VIS Microscope software data capture system (KERN and Sohn GmbH, Balingen, Germany) was used to take images of the samples.

6. COMPARATIVE STUDY OF THE POLYMORPHIC BEHAVIOUR OF CB, SHS AND THEIR BLENDS

The variation of cooling and heating rates influences the polymorphic behaviour of the samples. In this work, the studies were initiated using an intermediated rate of 2 ºC/min.

6.1. COOLING AND HEATING RATES OF 2 °C/MIN

6.1.1. Crystallization and polymorphic behaviour of pure samples

To understand the behaviour of blends based on CB and ShS, the polymorphic and crystallization behaviour of pure samples of CB and ShS were firstly studied. Figure 6 depicts the DSC thermograms and related XRD patterns of CB sample. Additionally, DSC data are summarised in the appendix 2, Table 3.

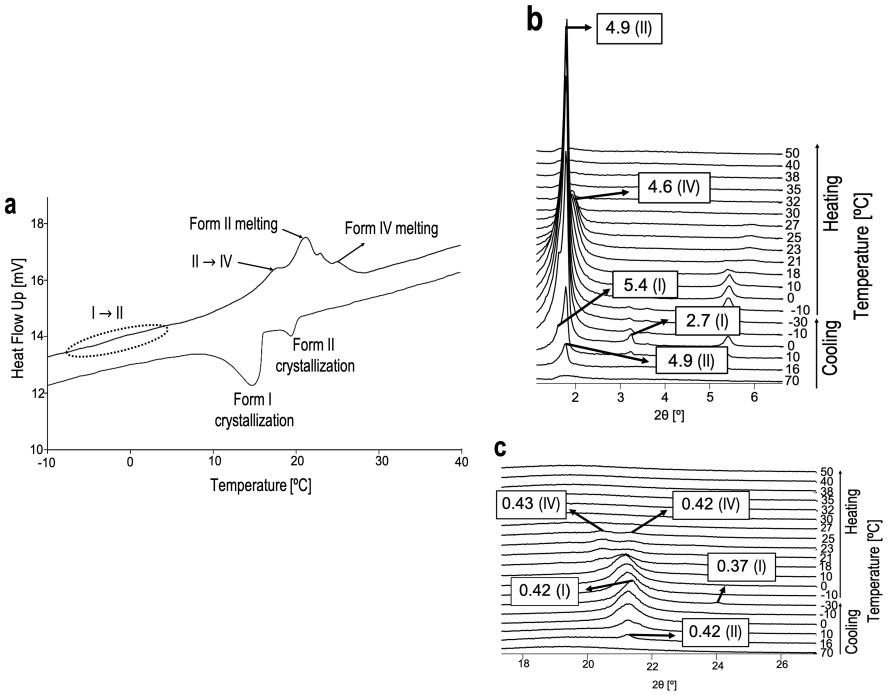

Figure 6. Polymorphic behaviour of CB when cooled and heated at 2 ºC/min: (a) DSC thermogram, and XRD small- (b) and wide- (c) angle region. D-spacing values are in nm.

During the cooling process, an exothermic peak was observed (T_{onset} = 20.1 $\pm$ 0.6 ºC). According to XRD data, this signal corresponded to the Form II crystallization, as typical small- and wide-angle peaks at 4.9 and 0.42 nm, respectively, were detected. Subsequently, DSC thermogram showed a second exothermic peak at 16.0 $\pm$ 0.4 ºC, which was assigned to Form I crystallization, as the XRD pattern revealed long spacing peaks at 5.4 and 2.7 nm.

When CB was subsequently heated, a broad and weak endothermic signal was detected in the range –5 to 5 ºC in the DSC, which was due to the transformation from Form I to Form II, as confirmed by XRD through the disappearance of small-angle diffraction peaks at 5.4 and 2.7 nm (Form I) and the increase of intensity of that at 4.9 nm (Form II). On further heating, the DSC thermogram showed an endothermic event at T_{onset} = 13.6 $\pm$ 0.3 ºC, which according to XRD data, was related to the transformation from Form II to Form IV. More specifically, at about 18 ºC, long and short spacing peaks at 4.9 and 0.42 nm (Form II), respectively, became less intense and then, at 21 ºC, a small-angle peak was detected at 4.6 nm (Form IV), accompanied by wide-angle peaks at 0.43 and 0.42 nm (Form IV). Soon after, Form II melted, as confirmed

by the disappearance of typical XRD peaks, and this phenomenon was assigned to a second endothermic event with T_{onset} = 17.7 $\pm$ 0.9 ºC. Finally, more stable Form IV also melted, which was associated to the last endothermic DSC signal with T_{top} = 24.9 $\pm$ 0.2 ºC.

These results obtained slightly differ from those reported by Bayés-García et al. [11], as they observed the occurrence of Form III, instead of Form IV at the same cooling and heating rates conditions. This fact may be due to the different XRD source used. Experiments performed by Bayés-García et al. [11] were carried out with synchrotron radiation source, which enables very rapid measurements while dynamic thermal treatments are applied. However, laboratory-scale XRD, which was used in the present work, involves longer measuring times and, consequently, a slight alteration of thermal treatments. This longer measuring time may have permitted the occurrence and stabilization of more stable Form IV, which was not detected by previous work.

Figure 7 shows the polymorphic and crystallization behaviour observed in ShS sample. Additionally, DSC data are shown in the appendix 2, Table 3.

α form was crystallized when ShS was cooled, as typical small- and wide-angle diffraction peaks at 5.2 and 0.42 nm, respectively, were identified at 22 ºC in corresponding XRD patterns. This crystallization was assigned to the first exothermic peak with T_{onset} = 25.0 $\pm$ 0.6 ºC. On further cooling, sub-α form crystallized at 21.4 $\pm$ 0.4 ºC, as according to XRD data, long spacing values of 5.5 and 2.7 nm were detected.

The broad and weak DSC peak in heating curve, between 0 to 10 ºC, corresponded to the transformation from sub-α form to α one. Then, the XRD small-angle region revealed a loss of intensity of peaks at 5.5 and 2.7 nm, and also of those in the wide-angle region at 0.42 and 0.38 nm (sub-α form). Soon after, the intensity of the α form peak at 5.2 nm increased. Subsequently, the DSC thermogram exhibited an endothermic signal with T_{top} = 19.5 $\pm$ 0.3 ºC, corresponding to the melting of α form, since XRD peaks with long and short spacing values of 5.2 and 0.42 nm (α form), respectively, disappeared at around 20 ºC. On further heating, a double exothermic event with T_{onset} = 20.2 $\pm$ 0.3 ºC was observed, which according to the XRD data, was due to the crystallization of γ form, identified through the long spacing peak at 3.7 nm and short spacing peaks at 0.47 and 0.39 nm. Finally, a broad endothermic phenomenon with T_{onset} = 29.4 $\pm$ 0.5 ºC occurred, and it was related to the melting of the previously crystallized γ form, as the XRD data revealed with the disappearance of its corresponding peaks.

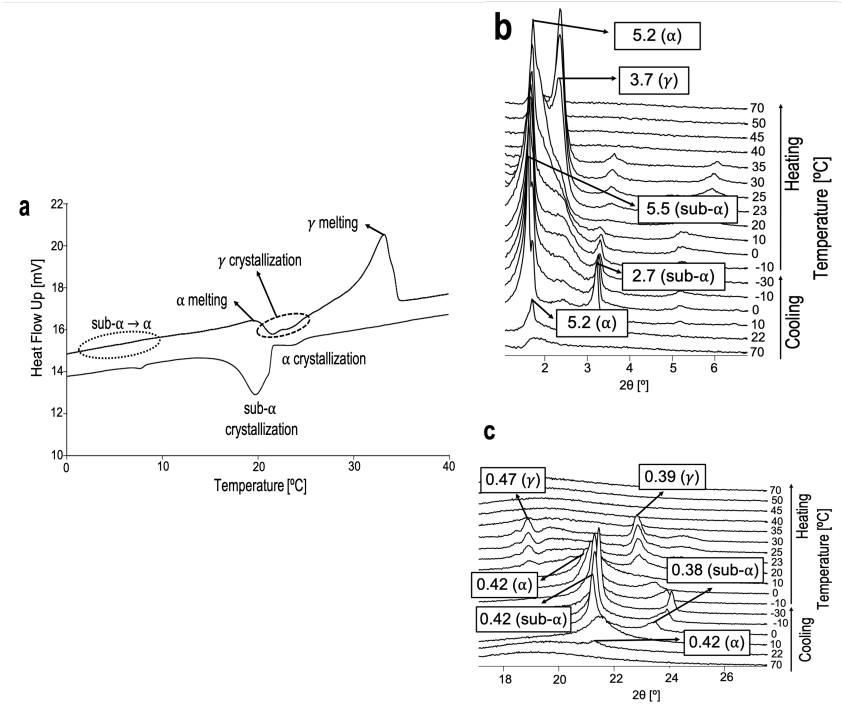

Figure 7. Polymorphic behaviour of ShS when cooled and heated at 2 ºC/min: (a) DSC thermogram, and XRD small- (b) and wide- (c) angle region. D-spacing values are in nm.

6.1.2. Crystallization and polymorphic behaviour of CB:ShS blends

DSC experiments were performed to analyse the crystallization and polymorphic behaviour of selected blends based on CB and ShS. Figure 8 depicts the DSC thermograms of all blends and pure samples of CB and ShS. Table 2 summarizes initial onset and final end temperatures for both cooling and heating processes.

At least three exothermic peaks appeared in the DSC cooling curves in the temperature range from 25 ºC to 0 ºC for all samples (peaks 1,3,4 in Figure 8a). Additionally, in pure ShS and mixtures from **B** to **E**, peak 3 exhibited one shoulder (peak 2). In general, DSC thermograms became highly similar for all samples, but all thermal events shifted to higher temperatures as the amount of ShS increased.

Regarding the heating step, four main endothermic signals were identified from 15 to 30 ºC in the CB sample and mixtures from **A** to **C** (peaks 5-8 in Figure 8b). Furthermore, samples of **D** and **E**, and pure ShS exhibited additional endothermic peaks from 22 to 35 ºC (peaks 5, 6 and

11). Additionally, the **E** mixture had one exothermic peak within the interval from 23 to 25 ºC (peak 12). In general, heating curves related to mixtures from **A** to **C** showed similar behaviour to that of CB sample, but thermal events became broader as the amount of CB decreased. From the **D** mixture and as ShS content increased, a broad endothermic peak occurred from 25 to 35 ºC. End and onset temperatures of the whole heating process increased with ShS concentration, as shown in Table 2.

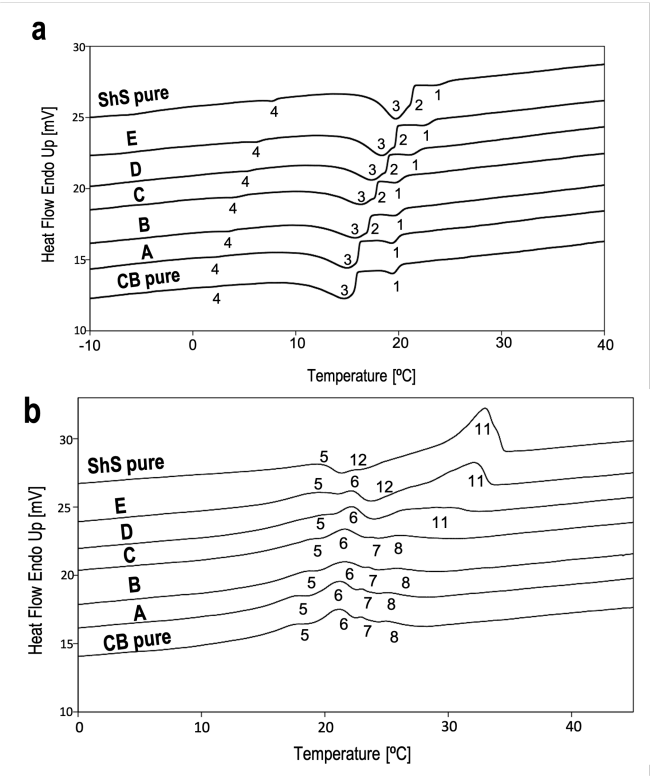

Figure 8. DSC cooling (a) and heating (b) thermograms of CB, ShS, and CB:ShS blends.

	Cooling (2ºC/min)		Heating (2ºC/min)	
Sample	T_{onset} [ºC]	T_{end} [ºC]	T_{onset} [ºC]	T_{end} [ºC]
CB	20.1 ± 0.6	9.6 ± 0.6	13.6 ± 0.3	27.4 ± 0.2
A	20.2 ± 0.4	10.3 ± 0.4	13.5 ± 0.5	27.7 ± 0.4
B	20.5 ± 0.4	10.8 ± 0.4	14.5 ± 0.6	28.6 ± 0.5
C	20.8 ± 0.3	11.7 ± 0.6	14.9 ± 0.7	29.5 ± 0.6
D	22.4 ± 0.4	13.3 ± 0.5	14.1 ± 0.2	32.2 ± 0.3
E	23.7 ± 0.3	14.8 ± 0.6	15.3 ± 0.6	33.5 ± 0.4
ShS	25.0 ± 0.6	16.7 ± 0.7	16.1 ± 0.4	34.7 ± 0.9

(a) T_{end} value corresponds to the second exothermic DSC peak.

Table 2. T_{onset} [ºC] and T_{end} [ºC] values for cooling and heating DSC curves.

Figure 9 shows the DSC and XRD data obtained corresponding to the **C** mixture. Additionally, DSC data of related thermal phenomena are shown in the appendix 2, Table 3.

During the cooling process, the DSC showed an exothermic peak at 20.8 ± 0.3 ºC, which, according to XRD data, corresponded to the crystallization of α form due to the occurrence of diffraction peaks at 5.0 and 0.42 nm. On further cooling, the DSC thermogram indicated the presence of a second exothermic peak with T_{onset} = 18.0 ± 0.3 ºC, which could be attributed to sub-α form crystallization (presence of diffraction peaks at 5.5, 2.7, 0.42 and 0.38 nm).

Regarding the subsequent heating stage, the DSC curve exhibited a broad and weak signal from about -5 to 5 ºC, corresponding to the transformation from sub-α form to α form (increase of intensity of diffraction peak at 5.0 nm at the expense of those at 5.5 and 2.7 nm). At higher temperatures, an intense endothermic DSC event with $T_{onset} \approx 14.9 \pm 0.7$ ºC was detected and it was attributed to the polymorphic transformation from α form to β'_{CB} and β'_{ShS} forms. In more detail, at ~20-23 ºC, the small-angle region peak at 5.0 nm (α form) disappeared and peaks at 4.6 nm (β'_{CB} form) and 3.5 nm (β'_{ShS} form) were detected. On further heating, a broad endothermic DSC peak with T_{top} = 26.0 ± 0.3 ºC appeared, corresponding to the concurrent melting of β'_{CB} and β'_{ShS} forms, as typical XRD peaks completely vanished at 32 ºC.

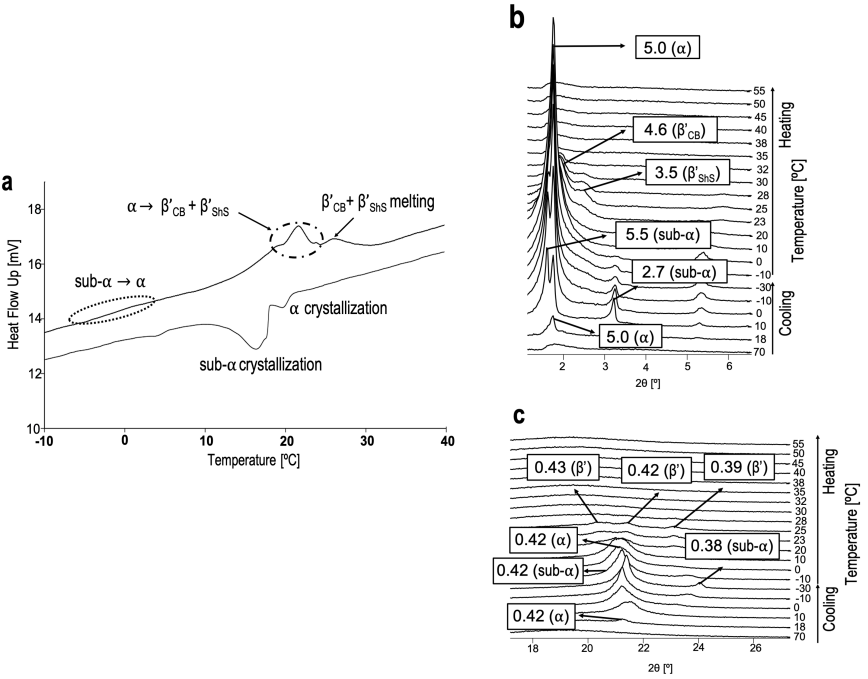

Figure 9. Polymorphic behaviour of the **C** blend when cooled and heated at 2 ºC/min: (a) DSC thermogram, and XRD small- (b) and wide- (c) angle region. D-spacing values are in nm.

Figure 10 displays the polymorphic behaviour of the **D** blend. Additionally, DSC data are indicated in appendix 2, Table 3.

When cooling the sample, the DSC thermogram showed a broad exothermic peak at 22.4 $\pm$ 0.4 ºC, due to the crystallization of α form, as typical long and short spacing peaks at 5.1 and 0.42 nm, respectively, were detected in XRD at 20 ºC. Another exothermic DSC event appeared at 19.1 $\pm$ 0.3 ºC, which corresponded to sub-α form crystallization (occurrence of diffraction peaks at 5.4, 2.7, 0.42 and 0.38 nm).

By reheating, the DSC thermogram again showed a broad and weak signal within the interval from -5 to 5 ºC, corresponding to the polymorphic transformation from sub-α to α form (decrease in the intensity of long spacing peaks at 5.4 and 2.7 nm of sub-α form, and increase of peak that at 5.0 nm, corresponding to α form). Simultaneously, in the wide-angle region, peaks at 0.42 and 0.38 nm (sub-α form) disappeared and a unique peak at 0.42 nm (α form) was observed. On further heating, the sequence of peaks detected by DSC may be related to a melt-mediated transformation from α form to β'_{CB} and β'_{ShS} forms. In more detail, an intense

endothermic peak accompanied by broad shoulder at ≈ 14.1 ± 0.2 ºC appeared in the corresponding DSC thermogram which was related to the melting of α form, as the XRD demonstrated with the disappearance of its typical peaks. Subsequently, an intense DSC signal with T_{top} = 24.1 ±0.3 ºC was assigned to the concurrent crystallization of β'_{CB} and β'_{ShS} forms, as XRD patterns exhibited small-angle diffraction peaks at 4.6 nm (β'_{CB} form) and 3.5 nm (β'_{ShS} form), and wide-angle diffraction peaks at 0.43, 0.42, and 0.39 nm (β' form). These β'_{CB} and β'_{ShS} forms melted almost concurrently at 24.2 ± 0.5 ºC.

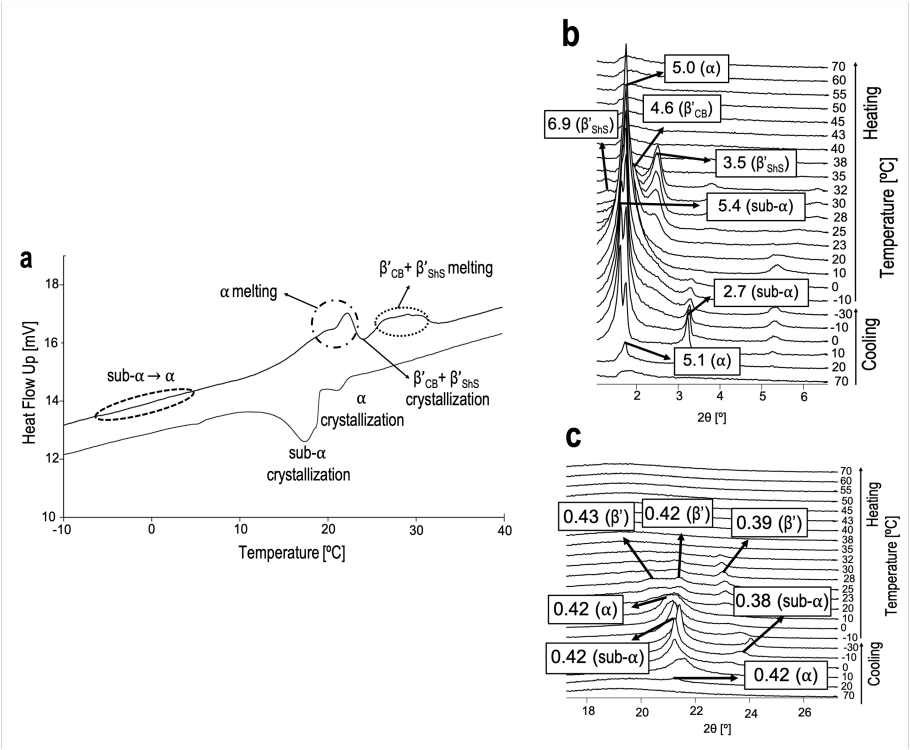

Figure 10. Polymorphic behaviour of the **D** blend when cooled and heated at 2 ºC/min: (a) DSC thermogram, and XRD small- (b) and wide- (c) angle region. D-spacing values are in nm.

One may note that the **D** blend had a similar polymorphic and crystallization behaviour compared with that of **C**. As expected, the amount of β'_{CB} form was higher in the **C** blend.

Figure 11 illustrates the polymorphic behaviour observed in the **E** blend and Table 3 in the appendix 2 shows the DSC data.

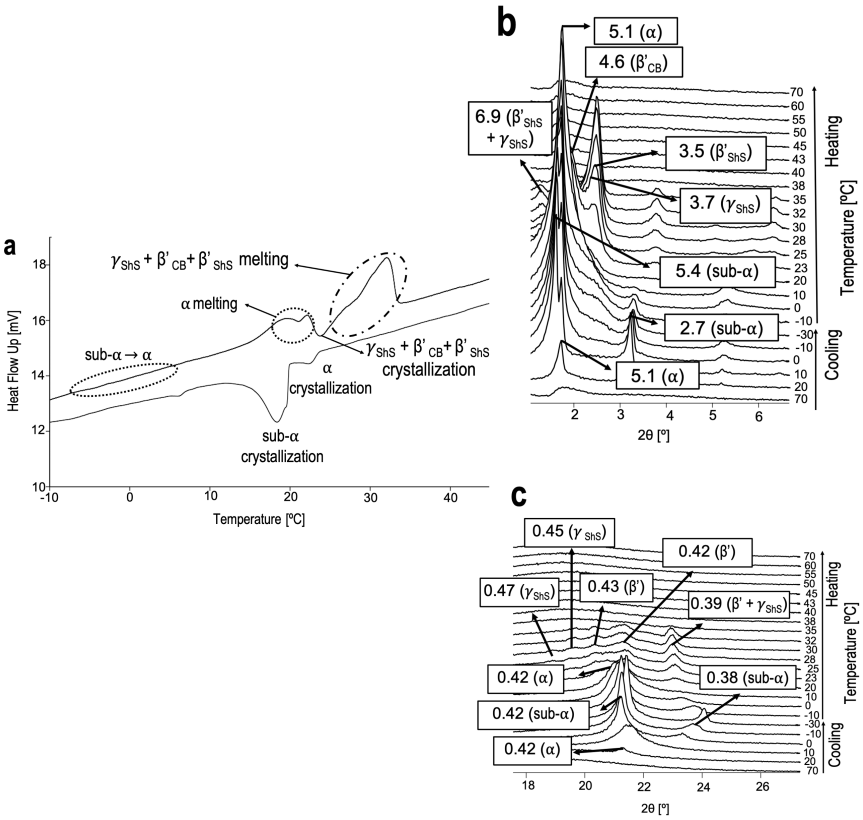

Figure 11. Polymorphic behaviour of the **E** blend when cooled and heated at 2 ºC/min: (a) DSC thermogram, and XRD small- (b) and wide- (c) angle region. D-spacing values are in nm.

When the **E** blend was cooled, an exothermic peak with T_{onset} = 23.7 $\pm$ 0.3 ºC was observed in the corresponding DSC cooling curve, which again was due to the crystallization of α form, as revealed by XRD peaks at 5.1 and 0.42 nm. An additional exothermic DSC peak appeared at 19.9 $\pm$0.3 ºC, which corresponded to sub-α form crystallization (small-angle peaks at 5.4 and 2.7 nm accompanied by wide-angle peaks at 0.42 and 0.38 nm).

By reheating the sample, again a broad and weak peak appeared from around -5 to 5 ºC in the DSC heating curve, which corresponded to the transformation from sub-α to α form. On further heating, α form melted, and this event was related to a double endothermic signal at 15.3 $\pm$0.6 ºC. Soon after, the DSC thermogram displayed an exothermic peak at 23.9 $\pm$ 0.6 ºC, which according to the XRD data, corresponded to the crystallization of β'_{CB} and β'_{ShS} forms. These were identified by diffraction peaks at 4.6 nm (β'_{CB} form) and 3.5 nm (β'_{ShS} form), and at

0.43 and 0.42 nm (β' form). Additionally, diffraction peaks at 3.7, 0.47, and 0.45 nm indicating the presence of γ_{ShS} form, were detected. Finally, all previously crystallized polymorphic forms melted at 27.2 ± 0.7 ºC, and typical XRD patterns completely disappeared at 32 ºC.

The **E** sample exhibited a very similar crystallization and polymorphic behaviour compared with those of **C** and **D**. However, in the **E** mixture, the presence of γ_{ShS} form was also detected, which was characteristic of ShS, and, as expected, the amount of β'_{CB} form was lower than β'_{ShS} form. To sum up, in Table 3 is shown the results obtained at 2 ºC/min.

	COOLING	HEATING
CB	Liquid $\xrightarrow{2\ ºC/min}$ **I + II**	$\xrightarrow{2\ ºC/min}$ **IV** $\longrightarrow$ Liquid
ShS	Liquid $\xrightarrow{2\ ºC/min}$ **sub-α + α**	$\xrightarrow{2\ ºC/min}$ **γ** $\longrightarrow$ Liquid
C	Liquid $\xrightarrow{2\ ºC/min}$ **sub-α + α**	$\xrightarrow{2\ ºC/min}$ **β'_{CB} + β'_{ShS}** $\longrightarrow$ Liquid
D	Liquid $\xrightarrow{2\ ºC/min}$ **sub-α + α**	$\xrightarrow{2\ ºC/min}$ **β'_{CB} + β'_{ShS}** $\longrightarrow$ Liquid
E	Liquid $\xrightarrow{2\ ºC/min}$ **sub-α + α**	$\xrightarrow{2\ ºC/min}$ **γ_{ShS} + β'_{CB} + β'_{ShS}** $\longrightarrow$ Liquid

Table 3. Polymorphic pathways of CB, ShS, and **C**, **D**, and **E** blends at 2 ºC/min.

Subsequently of the study at cooling/heating rates of 2 ºC/min, it was done another preliminary study at a lower rate of 0.5 ºC/min.

6.2. COOLING AND HEATING RATES OF 0.5 °C/MIN

The effects of varying cooling and heating rates on the crystallization and polymorphic behaviour of CB, ShS and selected blends of **C**, **D**, and **E** were also analysed. Then, lower rates of 0.5 ºC/min were employed.

6.2.1. Crystallization and polymorphic behaviour of pure samples

The crystallization and polymorphic behaviour of CB are shown in Figure 12. Additionally, DSC data are summarised in the appendix 2, Table 4.

Form II crystallized when CB was cooled, as long and short spacing peaks at 4.9 and 0.42 nm, respectively, were detected at 10 ºC. Simultaneously, the DSC cooling curve exhibited two exothermic peaks at T_{onset} = 21.4 ± 3.4 ºC and 16.3 ± 3.6 ºC.

When the sample was reheated, a broad and weak peak from around 10 to 20 ºC appeared in the corresponding DSC curve, due the polymorphic transformation from Form II to Form IV. According to XRD data, diffraction peak at 4.9 nm (Form II) disappeared, and, soon after, peaks at 4.6 and 0.43 nm (Form IV) occurred. This more stable polymorphic form completely melted at about 36 ºC, temperature at which no diffraction peaks were detectable.

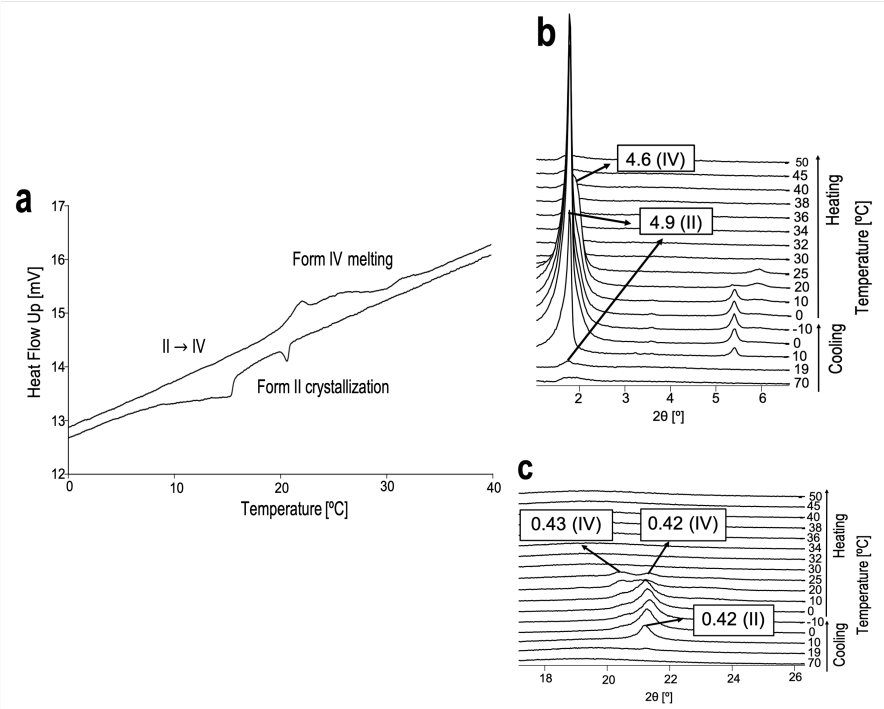

Figure 12. Polymorphic behaviour of CB when cooled and heated at 0.5 ºC/min: (a) DSC thermogram, and XRD small- (b) and wide- (c) angle region. D-spacing values are in nm.

The crystallization behaviour of CB when cooled and heated at 0.5 ºC/min slightly differed from that examined at 2 ºC/min, as least stable Form I did not occur at such low cooling rate. However, these results also differed from those reported by Bayés-García et al. [11], who did detect the occurrence of Form I of CB. As stated for cooling and heating conditions at 2 ºC/min, this may be due to the different XRD source used.

The crystallization and polymorphic behaviour of ShS are shown in Figure 13. In addition, DSC data of related thermal phenomena are summarised in the appendix 2, Table 4.

During the cooling process, the corresponding DSC curve exhibited a broad and weak exothermic peak at 27.0 ± 3.3 ºC, due to the α form crystallization, as XRD data revealed long and short spacing peaks at 5.1 and 0.42 nm, respectively. After that, the DSC cooling curve showed a double exothermic event at T_{onset}= 22.4 ± 2.4 ºC, which corresponded to the crystallization of β' form (occurrence of diffraction peaks at 3.6, 0.43, and 0.39 nm).

During the subsequent heating step, a broad and weak signal appeared in the DSC at around 20 ºC, which was related to the α form melting, as confirmed by XRD data through the disappearance of its typical peaks. Finally, the double endothermic event at 31.8 ± 0.4 ºC corresponded to the melting of β' form, since typical XRD peaks completely vanished at 42 ºC.

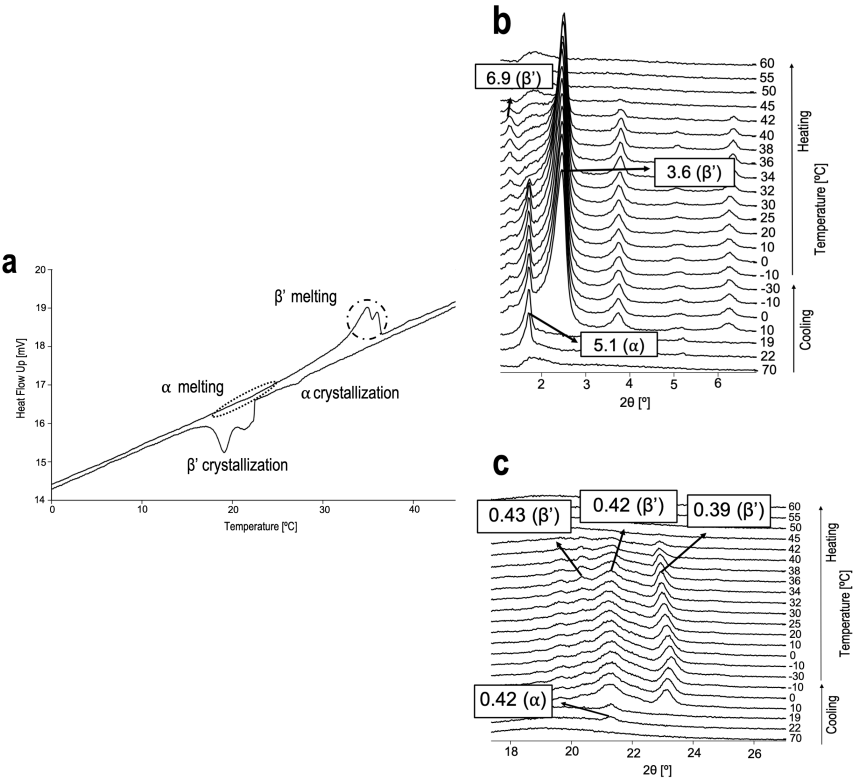

Figure 13. Polymorphic behaviour of the ShS when cooled and heated at 0.5 ºC/min: (a) DSC thermogram, and XRD small- (b) and wide- (c) angle region. D-spacing values are in nm.

A different polymorphic behaviour was determined when cooling/heating rates were decreased to 0.5 ºC/min. At such conditions, least stable sub-α form did not occur and more stable β' form was achieved. By contrast, by using higher rates of 2 ºC/min, γ form was obtained during heating, without further transformation to more stable phases. Hence, decreasing the cooling and heating rates allowed the stabilization of more stable polymorphic forms.

6.2.2. Crystallization and polymorphic behaviour of selected blends

Figure 14 shows the polymorphic and crystallization behaviour of **C** blend. Additionally, DSC data are summarised in the appendix 2, Table 4.

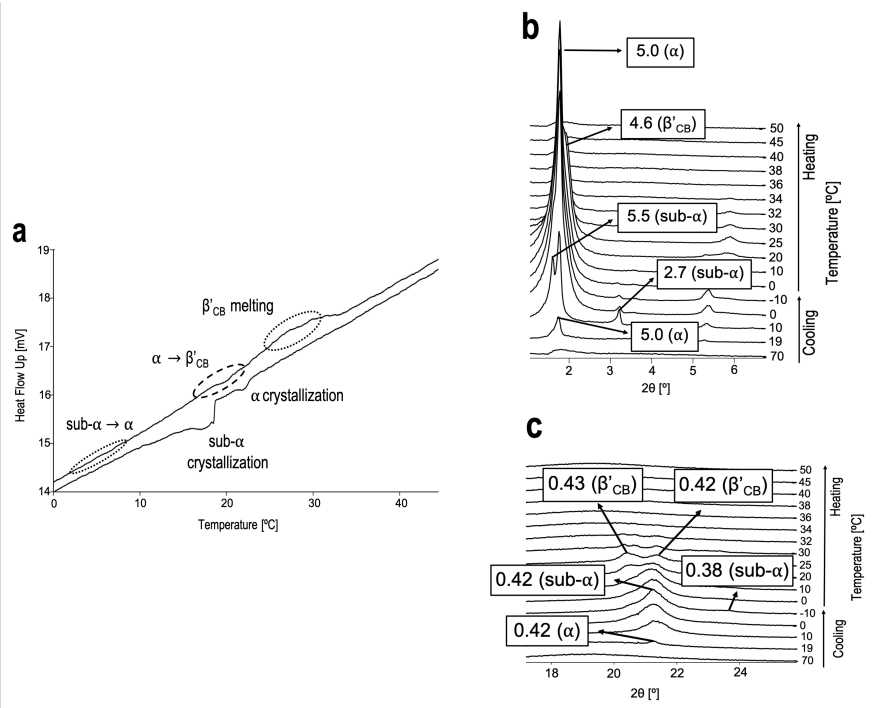

Figure 14. Polymorphic behaviour of the **C** blend when cooled and heated at 0.5 ºC/min: (a) DSC thermogram, and XRD small- (b) and wide- (c) angle region. D-spacing values are in nm.

α form crystallized when the **C** blend was cooled, as small- and wide-angle peaks at 5.0 and 0.42 nm, respectively, were observed. This process was related to the first thermal event detected in the DSC at 21.8 $\pm$ 2.5 ºC. Upon further cooling, the second thermal phenomenon at

18.4 ± 3.4 ºC was assigned to the crystallization of sub-α form, as XRD data revealed the occurrence of long spacing peaks at 5.5 and 2.7 nm and short-spacing value of 0.38 nm.

As to the heating stage, a polymorphic transformation from sub-α to α form occurred at around 5 ºC, as small-angle peaks at 5.5 and 2.7 nm (sub-α form) lost their intensity and, simultaneously, the long spacing peak at 5.0 nm (α form) became more intense. At a higher temperature of 17.6 ± 2.8 ºC, α form transformed into β'_{CB} (decrease of the intensity of α diffraction peak at 5.0 nm and occurrence of those of β'_{CB} at 4.6 and 0.43 nm). Finally, β'_{CB} form melted at about 22.9 ± 4.3 ºC, and no diffraction peaks were present at 34 ºC. One may note that, surprisingly, no β'_{ShS} form occurred when the **C** blend was cooled and heated at a lower rate of 0.5 ºC/min, as all β' form detected was that of CB.

Regarding the crystallization behaviour of the **D** blend, Figure 15 shows related DSC and XRD patterns, whereas thermal data are summarized in the appendix 2, Table 4.

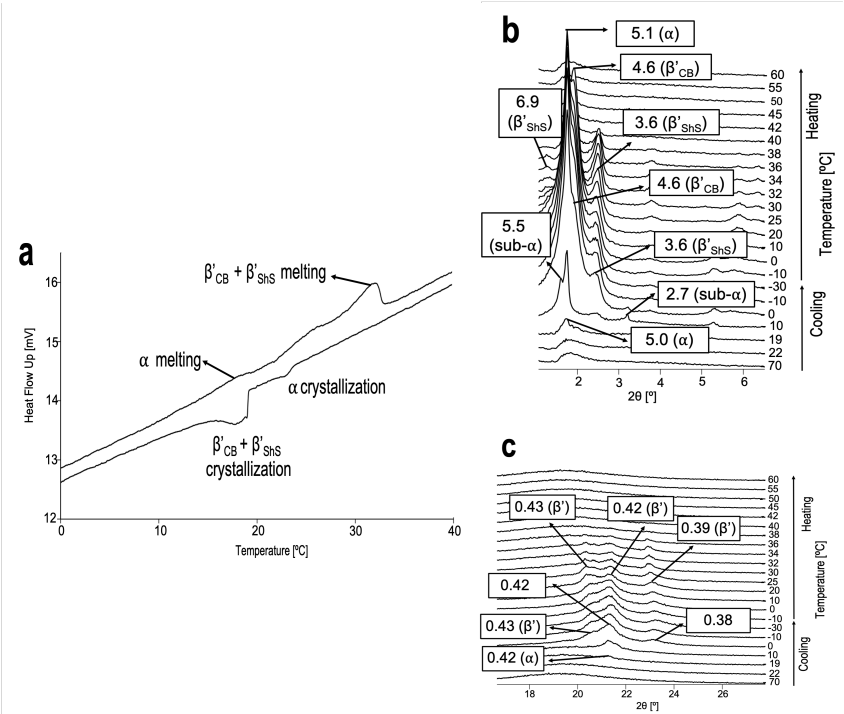

Figure 15. Polymorphic behaviour of the **D** blend when cooled and heated at 0.5 ºC/min: (a) DSC thermogram, and XRD small- (b) and wide- (c) angle region. D-spacing values are in nm.

When cooling the sample, the first exothermic peak observed in the DSC occurred at 23.8 $\pm$ 0.8 ºC, and it corresponded to the crystallization of α form, with typical small- and wide-angle diffraction peaks at 5.0 and 0.42 nm, respectively. At a lower temperature of 19.2 $\pm$ 0.5 ºC, the concurrent crystallization of β'_{CB} and β'_{ShS} took place, characterized by small-angle peaks at 3.6 nm (β'_{ShS} form) and 4.6 nm (β'_{CB} form) and wide-angle peaks at 0.43 and 0.42 nm. Additionally, at 10 ºC, the XRD data revealed the occurrence of metastable sub-α form, with its typical long spacing peaks at 5.5 and 2.7 nm, and soon after, at 0 ºC, these peaks vanished. By reheating the crystallized sample, polymorphic forms simply melted, without further transformations to more stable phases. Then, α form melted at first at 18.1 $\pm$ 1.4 ºC and, further on, β'_{CB} and β'_{ShS} forms melted almost concurrently at 31.8 $\pm$ 0.3 ºC.

The results obtained from DSC and XRD for sample **E**, (Figure 16 and Table 4 in appendix 2) suggested that its crystallization behaviour was similar to that of blend **D**.

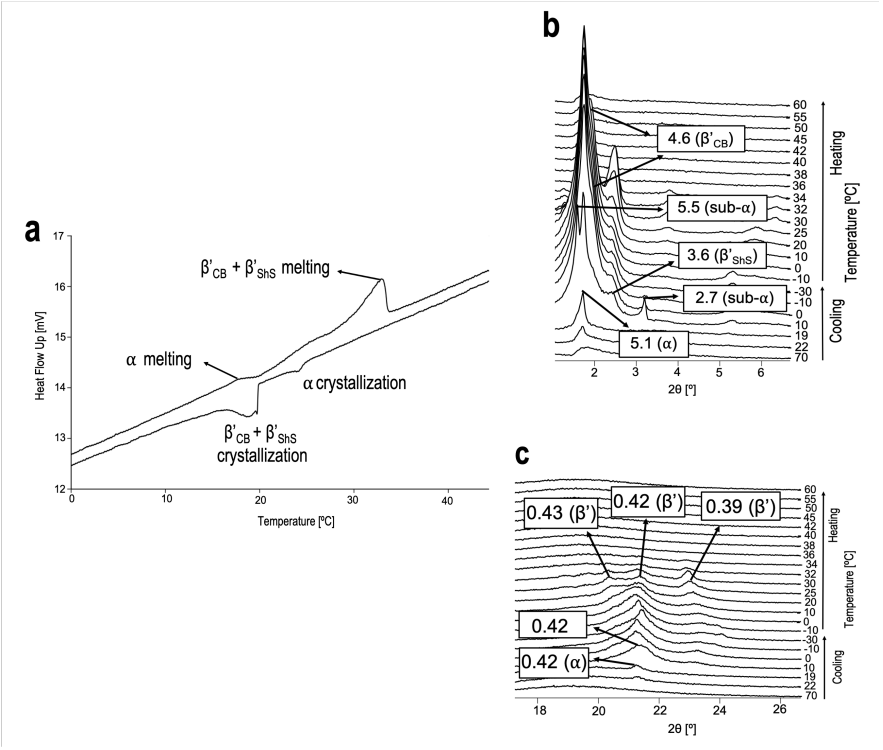

Figure 16. Polymorphic behaviour of the **E** blend when cooled and heated at 0.5 ºC/min: (a) DSC thermogram, and XRD small- (b) and wide- (c) angle region. D-spacing values are in nm.

When cooled from the melt, the sample crystallized at 24.3 ± 0.9 ºC into α form (X-ray diffraction peaks at 5.1 and 0.42 nm) and, on further cooling, the concurrent crystallization of β'_{CB} and β'_{ShS} forms occurred at 20.0 ± 0.3 ºC (3.6, 4.6, 0.43, and 0.39 nm). Again, transient sub-α form was detected at 10 ºC, as typical small-angle peaks at 5.5 and 2.7 nm were identified. However, as the temperature dropped to -30 ºC, this polymorphic form disappeared. When heating, previously crystallized forms simply melted: α form at 17.9 ± 1.1 ºC, and β'_{CB} and β'_{ShS} forms at about 33.1 ± 0.7 ºC.

A summary of the polymorphic crystallization and transformation behaviour of CB, ShS, and **C**, **D**, and **E** blends under varying conditions of cooling/heating is presented in Table 4. As already reported in previous work for single triacylglycerol components [13, 22, 23] and CB [11], less stable polymorphic forms predominated at higher rates, whereas the application of slower cooling and heating processes leaded the polymorphic crystallization and transformation to obtain more stable forms.

		COOLING	HEATING
CB	Liquid	2 ºC/min → I + II 0.5 ºC/min → II	2 ºC/min 0.5 ºC/min → IV → Liquid
ShS	Liquid	2 ºC/min → sub-α + α 0.5 ºC/min → α + β'	2 ºC/min → γ → Liquid 0.5 ºC/min → Liquid
C	Liquid	2 ºC/min 0.5 ºC/min → sub-α + α	2 ºC/min → β'_{CB} + β'_{ShS} → Liquid 0.5 ºC/min → β'_{CB} → Liquid
D	Liquid	2 ºC/min → sub-α + α 0.5 ºC/min → α + β'_{CB} + β'_{ShS}	2 ºC/min → β'_{CB} + β'_{ShS} → Liquid 0.5 ºC/min → Liquid
E	Liquid	2 ºC/min → sub-α + α 0.5 ºC/min → α + β'_{CB} + β'_{ShS}	2 ºC/min → γ_{ShS} + β'_{CB} + β'_{ShS} → Liquid 0.5 ºC/min → Liquid

Table 4. Polymorphic crystallization and transformation pathways of CB, ShS, and **C**, **D**, and **E** blends under different cooling/heating conditions.

In the CB sample, concurrent crystallization of Forms I and II occurred at a cooling rate of 2 ºC/min, whereas only Form II crystallized at a lower rate of 0.5 ºC/min. By contrast, at the heating stage, more stable Form IV was reached under both rates conditions.

Regarding ShS, the polymorphic behaviour exhibited at the different rates applied significantly differed. Concurrent crystallization of metastable sub-α and α forms occurred at 2 ºC/min, which transformed into γ form when heating at the same rate. By contrast, more stable β' form, together with α, crystallized at a lower cooling rate of 0.5 ºC/min. This forms simply melted when heating. Therefore, as expected, the decrease in cooling and heating rates allowed the occurrence of more stable polymorphic form, such as β'.

The polymorphic behaviour of **C**, **D**, and **E** mixtures subjected to cooling and heating rates of 2 ºC/min became highly similar. Nevertheless, the amount of β'_{ShS} increased at the expense of β'_{CB} as the concentration of ShS raised in the blend (from **C** to **E**), which was confirmed by the relative intensity of small-angle diffraction peaks in Figures 10-12. Furthermore, the blend including highest concentration of ShS (**E**) was the only one exhibiting the occurrence of γ_{ShS} form.

Regarding the cooling and heating rates variations, they did not cause significant changes in the **C** blend, containing highest amount of CB. However, the effects became more important as the amount of ShS increased in the blends. Then, for **D** and **E** mixtures, more stable β' forms of both CB and ShS were directly crystallized from the melt when cooled at 0.5 ºC/min, and sub-α form was not detected at such conditions. All phases simply melted when heated at 0.5 ºC/min.

The fact that mixtures with higher concentrations of ShS became more susceptible to the variations of the cooling and heating rates may be due to the difficulty exhibited by CB to achieve more stable forms by modifying dynamic thermal treatments compared to other fat systems [13, 22, 23]. These factors may be carefully taken into account when determining the necessary conditions for the design of lipid products with desired physicochemical characteristics.

7. SOLID FAT INDEX

The Solid fat index (SFI) of a lipid system shows the variation of the solid content as a function of temperature and it becomes a useful tool to determine the functional characteristics of edible fats [24]. In this study, the determination of SFI for all the samples was performed from the partial areas analyses of corresponding DSC heating curves.

As shown in Figure 17, CB and mixtures containing highest amount of CB (**A** and **B**) exhibited a one-stage SFI variation, in which samples were 100% solid at around 13 ºC, SFI dropped drastically from above 15 ºC, and the solid content was about 0% at a temperature below 30 ºC. This unique sharp melting behaviour is typical of CB and the responsible for the characteristic organoleptic properties and strong flavour release of chocolate.

In contrast, for blends of **C**, **D**, and **E** and pure ShS, SFI dropped in two different stages (the first one ending at 25 ºC), and this differentiation became more pronounced as the content in ShS increased in the blends. Furthermore, the melting profile became flatter for mixtures with higher ShS percentage, so that melting started at lower temperatures and finished at higher temperatures. Then, the addition of ShS to CB caused an increase in solid fat percentage, and higher melting temperature and hardness.

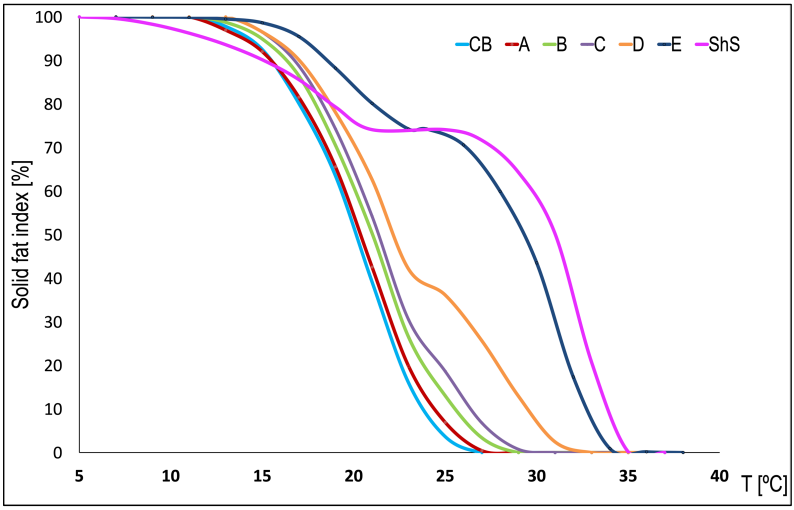

Figure 17. SFI of all the samples.

8. POLARIZED LIGHT MICROSCOPY

Polarized light microscopy (PLM) is a technique that allows the visualization of textural differences, morphological variations related to crystal growth, and polymorphic transformations of fats [14]. Besides, the study of microstructures in fats is essential to understand the macroscopic properties of fats and fat-containing products, which depend on their fat crystal network [9]. In this study, PLM was used to characterize the microstructure of CB, ShS, and selected blends of **C** and **D**, which were crystallized at 22 ºC for 1 to 40 days. The temperature of 22 ºC was selected to avoid the occurrence of less stable polymorphic forms. Specific XRD experiments allowed to relate crystal morphology and polymorphism.

8.1. CRYSTAL MORPHOLOGY AND POLYMORPHISM OF CB AND SHS

Figure 18 depicts polarized light microscopy images of CB microstructure, taken from 1 to 40 days of incubation at 22 ºC. Figure 19 shows complementary XRD data.

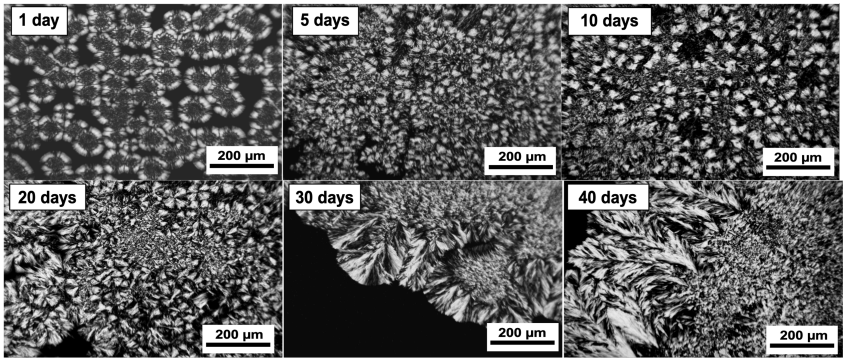

Figure 18. PLM images of CB thermodynamic stabilised at 22 ºC for a certain time.

After 1 day of incubation at 22 ºC, small spherulite-like crystal aggregates (~100 µm) were observed (Figure 18), which according to XRD data, corresponded to Form IV of CB (Figure 19). Although no significant changes in crystal morphology or size were detected by PLM after 5 and 10 days of incubation, corresponding XRD patterns revealed the occurrence of more stable Form V of CB, which may have formed through polymorphic transformation from Form IV. However, after 20 days of thermodynamic stabilization at 22 ºC, PLM revealed the presence of large feather-like crystals at the periphery of crystal aggregates. These crystals became more important as incubation time increased, predominating after 40 days of incubation. According to related XRD data, only Form V was present in the sample after 10 days of incubation.

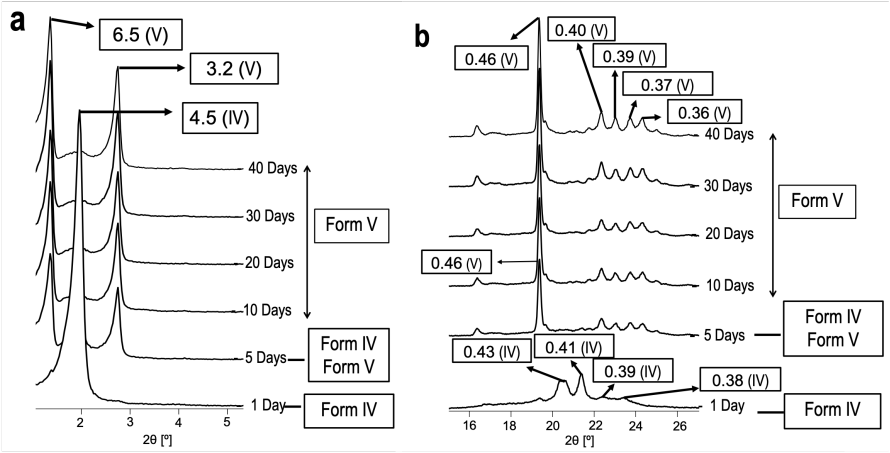

Figure 19. XRD pattern of CB: small- (a) and wide-(b) angle region. D-spacing values are in nm.

Figure 20 shows polarized microscopy images of the ShS microstructure from 1 to 40 days at 22 ºC, whereas corresponding XRD patterns are presented in Figure 21.

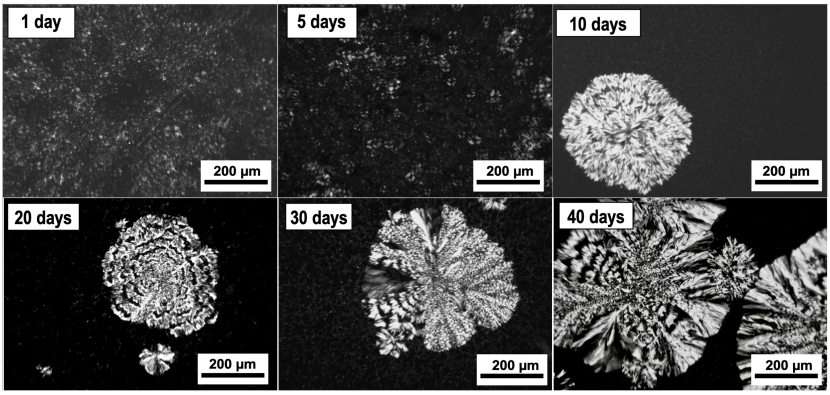

Figure 20. PLM images of ShS statically crystallized at 22 ºC for certain time.

Small (~ 40 µm) spherulitic crystals aggregates were observed after 1 and 5 days of incubation at 22 ºC (Figure 20), which, based on XRD data, were related to γ and β' forms of ShS (Figure 21). After 10 days, a large microstructure with a featherlike appearance (~ 500 µm) was observed. This crystal morphology was formed due to a polymorphic transformation from less stable γ and β' forms to more stable β form, and it increased in quantity and size as days went by. After 20 days, γ form disappeared and just β' and β forms coexisted, and only β was present after 40 days, moment at which crystal aggregates composed by feather-like crystals were about 800 µm diameter.

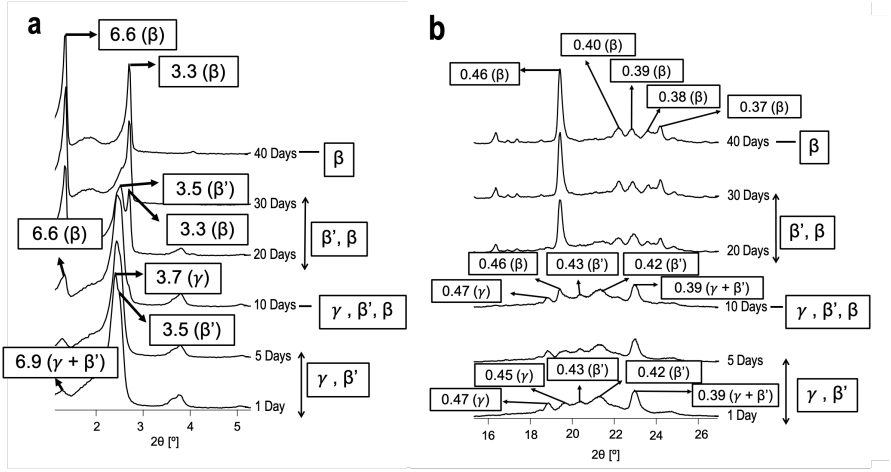

Figure 21. XRD pattern of ShS: small- (a) and wide-(b) angle region. D-spacing values are in nm.

8.2. CRYSTAL MORPHOLOGY AND POLYMORPHISM OF SELECTED BLENDS

Figure 22 shows polarized microscopy images of the **C** blend when subjected to thermodynamic stabilization at 22 ºC. Related small- and wide-angle region XRD data are presented in Figure 23.

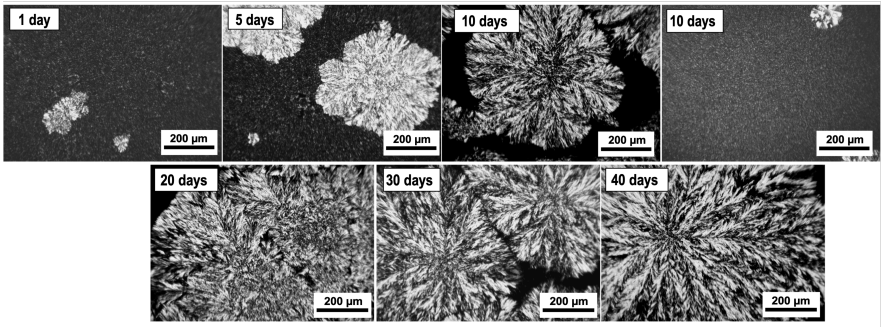

Figure 22. PLM images of **C** blend at certain days of storage at 22 ºC.

After 1 day of storage at 22 ºC, granular morphology crystals with co-existing spherulites of about 100 nm diameter were detected (Figure 22). According to the XRD data, concurrent crystallization of β' form of CB and ShS, and most stable β of CB and ShS occurred (Figure 23). After 5 days, spherulitic aggregates grew (~ 650 µm) and adopted a featherlike appearance. These morphological changes may be related to the completion of the transformation from β' form of CB and ShS to their most stable β forms. From the 10th to 40th day, only β crystals were

present, and they significantly increased their size, and, around them, a continuous granular morphology was observed. However, larger feather-like crystals made difficult their differentiation.

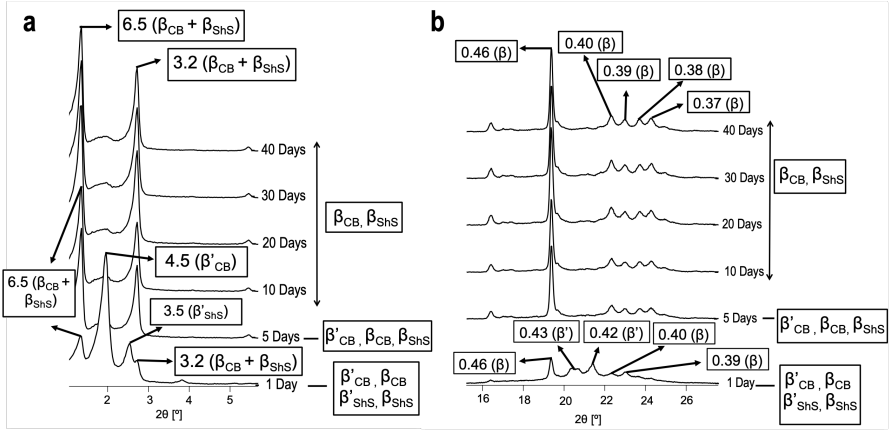

Figure 23. XRD data of **C** blend: small- (a) and wide-(b) angle region. D-spacing values are in nm.

Figure 24 and 25 show PLM images of the **D** microstructure, obtained from 1 to 40 days at 22 ºC, and XRD patterns at the same experimental conditions, respectively.

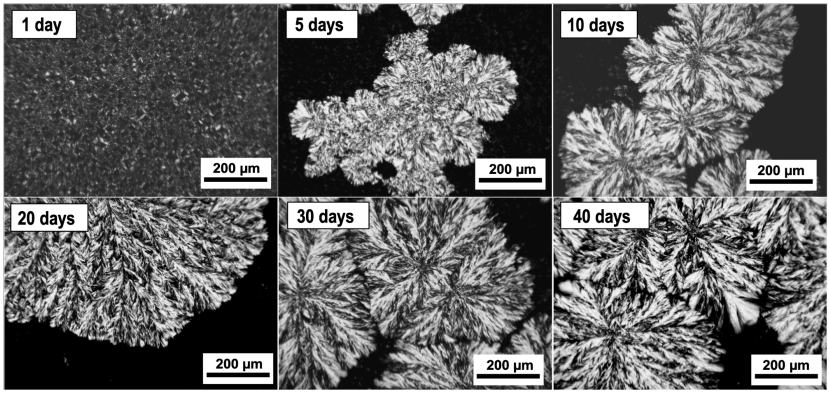

Figure 24. PLM images of **D** blend statically crystallized at 22 ºC at certain time.

After 1 day of incubation at 22 ºC, granular morphology with some tiny spherulitic aggregates were observed (Figure 24). Simultaneously, corresponding XRD pattern revealed the occurrence of β' forms of CB and ShS and most stable β forms of CB and ShS (Figure 25). Then, as days went by, β' forms transformed into most stable β forms for both CB and ShS. This

transformation again coincided with the occurrence of large spherulites formed by feather-like crystals (~ 500 μm).

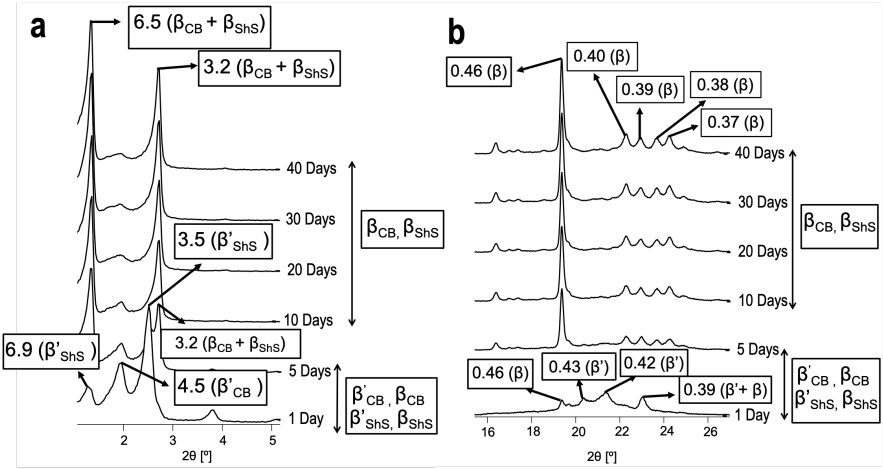

Figure 25. XRD data of **D** blend: XRD small- (a) and wide-(b) angle region. D-spacing values are in nm.

In conclusion, the results obtained from these studies reveal that CB exhibited a higher tendency to stabilize in Form V (β form) than ShS: for CB this was the only polymorphic form present after 10 days of incubation, whereas ShS needed 40 days to completely stabilize. This fact may be due to the higher melting temperatures of polymorphic forms of ShS and the consequent need of higher temperatures to settle more stable forms. Then, the presence of CB in ShS reduced the stabilization time of ShS in most stable β form. The two blends of CB and ShS were in their most stable β forms just after 10 days of incubation, and their occurrence were related to the growth of large feather-like crystals in spherulitic aggregates. Furthermore, metastable γ form of ShS was not detected in the blends. By comparing the two blends analysed, one may note that in the **C** sample, all ShS was in its most stable β form after 5 days of incubation, whereas β' form was still present in the **D** mixture, which may be due to the higher amount of CB present in the former case.

9. CONCLUSIONS

The conclusions which can be extracted from this work are the following:

- The polymorphic behaviour of CB, ShS, and five CB:ShS mixtures in ratios 95:5, 80:20, 70:30, 50:50, and 30:70 (blends **A** to **E**, respectively) were studied. In specific, CB, ShS, and **C**, **D**, and **E** blends were analysed with DSC and XRD under different dynamic conditions of varied cooling/heating rates. The results indicated that less stable polymorphic forms were detected when high rates were applied, whereas more stable phases predominated at lower rates. More stable β' form of CB and ShS were identified in all the mixtures. Additionally, γ form was a polymorphic form characteristic of shea stearin.

- The solid fat index as a function of temperature was studied for CB, ShS, and **A** to **E** blends. CB and mixtures containing highest amounts of CB exhibited a sharp melting profile based on one-stage SFI variation, whereas SFI of ShS and samples rich in ShS dropped more gradually and in two clear stages. Then, the addition of ShS to CB caused a flatter melting profile, increase in solid fat percentage, and higher melting temperature and hardness.

- The microstructure and polymorphism of CB, ShS, and **C** and **D** blends were investigated with PLM and complementary XRD. CB exhibited a higher tendency to stabilize in Form V (β form) than ShS, so that the presence of CB in the blends enabled the stabilization of ShS in its most stable β form. The two CB:ShS blends analysed were in their most stable β forms just after 10 days of incubation at 22 ºC, and their occurrence were related to the growth of larger feather-like crystals in spherulitic aggregates.

- The application of external factors to lipid systems, such as the addition of a second component or the use of dynamic thermal treatments with varied cooling/heating rates may permit the design of functional products with desired physicochemical characteristics (melting behaviour, hardness) for specific applications. In this work, we determined how the additions of ShS may modify the crystallization and polymorphic behaviour of CB, and these effects may be intensified by tuning the experimental conditions used (e.g. specific dynamic thermal treatments).

10. REFERENCES AND NOTES

1. Bernstein, J. In *Polymorphism in Molecular Crystals*; Oxford University Press: New York, USA, 2020.
2. Larsson, K.; Quinn, P.; Sato, K.; Tiberg, F. In *Lipids: Structure, physical properties, and functionality*; The Oily Press: Bridgewater, USA, 2006.
3. Marangoni, A.G.; Narine, S.S. In *Physical Properties of Lipids*; Marcel Deker: New York, USA, 2002.
4. Sato, K. Polymorphism of Lipid Crystals. In *Crystallization of Lipids: Fundamentals and Applications in Food, Cosmetics, and Pharmaceuticals.* Sato, K., Ed.; Wiley Blackwell: West Sussex, UK, 2018; p 17-61.
5. Bootello, M.A.; Hartel, R.W.; Garcés, R.; Martínez-Force, E.; Salas, J.J. Evaluation of high oleic-high stearic sunflower hard stearins for cocoa butter equivalent formulation. *Food Chem*. **2012**, 134,1409-1417.
6. Verstringe, S.; de Clercq., N.; Nguyen, T.M.; Kadivar, S.; Dewettinck, K.; Enzymatic and Other Modification Techniques to Produce Cocoa Butter Alternatives. In *Cocoa Butter and Related Compounds*. Garti, N., Widlak, N.R., Ed.; AOCS Press:Urbana, Illinois, USA, **2012,** p 443-474.
7. Timms, R.E. In *Confectionery fats handbook: properties, production, and application*. The Oily Press: Bridgwater, UK, 2003.
8. Wille R.L.; Lutton, E.S. Polymorphism of Cocoa Butter. *J. Am. Oil. Chem. Soc.* **1966**, 43, 491- 496.
9. Marangoni, A.G; McGauley, S.E. Relationship between Crystallization Behaviour and Structure in Cocoa Butter. *Cryst. Growth Des*. **2003**, 3, 95-108.
10. Bayés-García, L.; Calvet, T.; Cuevas-Diarte, M.A.; Rovira, E.; Ueno, S.; Sato, K. New Textures of Chocolate Are Formed by Polymorphic Crystallization and Template Effects: Velvet Chocolate. *Cryst. Growth Des.* **2015**, 15, 4045-4054.
11. Bayés-García, L.; Aguilar-Jiménez, M.; Calvet, T.; Koyano, T.; Sato, K. Crystallization and Melting Behaviour of Cocoa Butter in Lipid Bodies of Fresh Cacao Beans. *Cryst. Growth Des.* **2019**, 19, 4127-4137.
12. Ueno, S.; Minato, A.; Seto, H.; Amemiya, Y.; Sato, K. Synchrotron X-ray Diffraction Study of Liquid Crystal Formation and Polymorphic Crystallization of SOS (*sn*-1,3-Diestearoyl-2-oleoyl Glycerol). *J. Phys. Chem. B.* **1997**, 101, 6847-6854.
13. Bayés-García, L.; Calvet, T.; Cuevas-Diarte, M.A.; Ueno, S.; Sato, K. *In situ* observation of transformation pathways of polymorphic forms of 1,3-dipalmitoyl-2-oleoyl glicerol (POP) examined with synchrotron radiation X-ray diffraction and DSC. *Cryst. Eng. Comm.* **2013,** 15, 302-314.
14. Ray, J.; Smith, K.W.; Bhaggan, K.; Nagy, K.Z.; Stapley, A.G.F. Crystallization and polymorphic behaviour of shea stearin and the effect of removal of polar components. *Eur. J. Lipid Sci. Technol.* **2013**, 115, 1094-1106.
15. Kang, K.K.; Jeon, H.; Kim, I-H; Kim, B.H. Cocoa Butter Equivalents Prepared by Blending Fractionated Palm Stearin and Shea Stearin. *Food. Sci. Biotechnol.* **2013**, 22, 347-352.
16. Zeng, J.; Shen, J.; Wu, Y.; Liu, X.; Deng, Z-Y.; Li, J. Effect of adding shea butter stearin and emulsifiers on the physical properties of cocoa butter. *J. Food Sci.* **2020**, 85, 972-979.
17. Larsson, K. On the structure of the liquid state of triglycerides. *J. Am. Oil. Chem. Soc*. **1992**, 69, 835-836.
18. Small, D.M. In *The Physical Chemistry of Lipids*; Plenum: New York, USA, 1986; p 345-394.
19. Sato, K. In *Advances in Applied Lipid Research*; Padley, F., Ed; JAI Press Inc: 1996; Vol. 2; p 213-268.

20. Sato, K. Molecular Aspects in Fat Polymorphism. In *Crystallization and Solidification Properties of Lipids;* Widlak, N., Hartel, R., Narine, S., Ed; AOCS Press: Champaign, Illinois, USA, 2001, p 1-17.
21. Perkin Elmer. Instructions Model DSC-4. Norwalk, Connecticut, USA, **1982**.
22. Bayés-García, L.; Calvet, T.; Cuevas-Diarte, M.A.; Ueno, S.; Sato, K. Crystallization and Transformation of Polymorphic Forms of Trioleoyl Glycerol and 1,2-Dioleoyl-3-*rac*-linoleoyl Glycerol. *J. Phys. Chem. B.* **2013,** 117, 9170-9181.
23. Bayés-García, L.; Calvet, T.; Cuevas-Diarte, M.A.; Ueno, S. *In situ* crystallization and transformation kinetics of polymorphic forms of saturated-unsaturated-unsaturated triacylglycerols: 1-palmitoyl-2,3-dioleoyl glycerol, 1-stearoyl-2,3-dioleoyl glycerol, and 1-palmitoyl-2-oleoyl-3-linoleoyl glycerol. *Food Res. Int.* **2016,** 85, 244-258.
24. van de Voort, F.R.; Memon, K.P.; Sedman, J.; Ismail, A.A. Determination of Solid Fat Index by Fourier Transform Infrared Spectroscopy. *J. Am. Oil. Chem. Soc.* **1996**, 73, 411-416.

11. ACRONYMS

CB: Cocoa Butter

CBA: Cocoa Butter Alternative

CBE: Cocoa Butter Equivalent

CBEX: Cocoa Butter Extender

CBI: Cocoa Butter Improver

CBR: Cocoa Butter Replacer

CBS: Cocoa Butter Substitute

DAG: Diacylglycerol

DSC: Differential Scanning Calorimetry

PLM: Polarized Light Microscopy

POP: 1,3-dipalmitoyl-2-oleoyl-glycerol

POS: *rac*-palmitoyl-stearoyl-2-oleoyl-glycerol

SFC: Solid Fat Content

SFI: Solid Fat Index

ShS: Shea Stearin

SOS: 1,3-distearoyl-2-oleoyl-glycerol

TAG: Triacylglycerol

TPA: Texture Profile Analysis

XRD: X-ray Diffraction

APPENDICES

APPENDIX 1: TABLES OF CB AND SOS POLYMORPHS

Polymorphic form	Equivalence	T_m [ºC]	Long spacing [nm]	Short spacing [nm]
I	sub-α	17.3	5.45	0.419 (vs), 0.370 (s)
II	α	23.3	4.9	0.424 (vs)
III	β'_2	25.5	4.9	0.462 (w), 0.425 (vs), 0.386 (s), 0.462 (w)
IV	β'_1	27.5	4.5	0.435 (vs), 0.415 (vs), 0.397 (m), 0.381 (m)
V	β_2	33.8	6.38	0.54 (m), 0.515 (w), 0.458 (vs), 0.423 (vvw), 0.398 (s), 0.387 (m), 0.375 (m), 0.367 (w), 0.330 (vw)
VI	β_1	36.3	6.41	0.543 (m), 0.515 (w), 0.459 (vs), 0.427 (vw), 0.404 (w), 0.386 (m), 0.370 (s), 0.336 (vw)

a) The relative intensity is indicated as very strong (vs), strong (s), medium (m), weak (w), very weak (vw) and very very weak (vvw).

Table 1. Typical XRD values and T_m of polymorphic forms of CB [8].

Polymorphic form	T_m [ºC]	Long spacing [nm]	Short spacing [nm]
α	23.3	4.83	0.421 (vs)
γ	35.4	7.05	0.472 (s), 0.450 (m), 0.388 (s)
β'	36.5	7.00	0.430 (m), 0.415 (m), 0.402 (s), 0.396 (m)
β_2	41.0	6.50	0.458 (vs), 0.400 (m), 0.390 (m), 0.375 (m), 0.367 (m),
β_1	43.0	6.50	0.458 (vs), 0.402 (w), 0.397 (w), 0.385 (w), 0.380 (w)

a) The relative intensity is indicated as very strong (vs), strong (s), medium (m), weak (w) and very weak (vw).

Table 2. Typical XRD values and T_m of polymorphic forms of SOS [12].

APPENDIX 2: TABLES OF DSC DATA UNDER DIFFERENT COOLING/HEATING CONDITIONS

Sample	Thermal treatment	Polymorphic form	Temperature [ºC]	
CB	Cooling	Form II crystallization	Onset = 20.1 ± 0.6	End = 17.6 ± 0.6
		Form I crystallization	Onset = 16.0 ± 0.4	End = 9.6 ± 0.6
	Heating	Form I → Form II	Could not determined	
		Form II → Form IV	Onset = 13.6 ± 0.3	Top = 17.6 ± 0.3
		Form II melting	Onset = 17.7 ± 0.9	Top = 20.9 ± 0.5
		Form IV melting	Top = 24.9 ± 0.2	
ShS	Cooling	α crystallization	Onset = 25.0 ± 0.6	End = 21.0 ± 0.4
		sub-α crystallization	Onset = 21.4 ± 0.4	End = 16.7 ± 0.7
	Heating	sub-$\alpha \rightarrow \alpha$	Could not determined	
		α melting	Top = 19.5 ± 0.3	End = 20.2 ± 0.3
		γ crystallization	Onset = 20.2 ± 0.3	End = 24.3 ± 0.8
		γ melting	Onset = 29.4 ± 0.5	End = 34.7 ± 0.9
C	Cooling	α crystallization	Onset = 20.8 ± 0.3	End = 17.2 ± 0.5
		sub-α crystallization	Onset = 18.0 ± 0.3	End = 11.7 ± 0.6
	Heating	sub-$\alpha \rightarrow \alpha$	Could not determined	
		$\alpha \rightarrow \beta'_{CB} + \beta'_{ShS}$	Top = 14.9 ± 0.7	End = 24.3 ± 0.3
		$\beta'_{CB} + \beta'_{ShS}$ melting	Onset = 26.0 ± 0.3	End = 29.5 ± 0.6
	Cooling	α crystallization	Onset = 22.4 ± 0.4	End = 18.5 ± 0.5

D		sub-α crystallization	Onset = 19.1 ± 0.3	End = 13.3 ± 0.5
	Heating	sub-α → α	Could not determined	
		α melting	Onset = 14.1 ± 0.2	End = 23.7 ± 0.8
		β'_{CB} + β'_{ShS} crystallization	Top = 24.1 ± 0.3	
		β'_{CB} + β'_{ShS} melting	Onset = 24.2 ± 0.5	End = 32.2 ± 0.3
E	**Cooling**	α crystallization	Onset = 23.7 ± 0.3	End = 20.2 ± 0.6
		sub-α crystallization	Onset = 19.9 ± 0.3	End = 14.8 ± 0.6
	Heating	sub-α → α	Could not determined	
		α melting	Onset = 15.3 ± 0.6	End = 23.0 ± 0.3
		γ_{ShS} + β'_{CB} + β'_{ShS} crystallization	Top = 23.9 ± 0.6	
		β'_{CB} + β'_{ShS} melting	Onset = 27.2 ± 0.7	End = 33.5 ± 0.4

Table 3. DSC cooling (2ºC/min) and heating (2ºC/min) data for CB, ShS, and **C**, **D**, and **E** blends.

Sample	**Thermal treatment**	**Polymorphic form**	**Temperature** [ºC]	
CB	**Cooling**	Form II crystallization	Onset = 21.4 ± 3.4 (peak 1)	Onset = 16.3 ± 3.6 (peak 2)
	Heating	Form II → Form IV	Could not determined	
		Form IV melting	Onset = 30.5 ± 5.6	End = 33.9 ± 5.9
ShS	**Cooling**	α crystallization	Top = 27.0 ± 3.3	
		β' crystallization	Onset = 22.4 ± 2.4	End = 18.2 ± 9.2
	Heating	α melting	Could not determined	
		β' melting	Onset = 31.8 ± 0.4	End = 36.3 ± 3.1
C	**Cooling**	α crystallization	Top = 21.8 ± 2.5	
		sub-α crystallization	Onset = 18.4 ± 3.4	
	Heating	sub-α → α	Could not determined	

		$\alpha \rightarrow \beta'_{CB}$	Top = 17.6 $\pm$ 2.8	
		β'_{CB} melting	Onset = 22.9 $\pm$ 2.8	End = 32.8 $\pm$ 0.5
D	**Cooling**	α crystallization	Top = 23.8 $\pm$ 0.8	
		β'_{CB} + β'_{ShS} crystallization	Onset = 19.2 $\pm$ 0.5	
	Heating	α melting	Top = 18.1 $\pm$ 1.4	
		β'_{CB} + β'_{ShS} melting	Top = 31.8 $\pm$ 0.3	End = 33.0 $\pm$ 0.4
E	**Cooling**	α crystallization	Top = 24.3 $\pm$ 0.9	
		β'_{CB} + β'_{ShS} crystallization	Onset = 20.0 $\pm$ 0.3	
	Heating	α melting	Top = 17.9 $\pm$ 1.1	
		β'_{CB} + β'_{ShS} melting	Top = 33.1 $\pm$ 0.7	End = 33.9 $\pm$ 1.4

Table 4. DSC cooling (0.5 ºC/min) and heating (0.5 ºC/min) data for CB, ShS, and **C**, **D** and **E**.